Journal of Materials Chemistry A

ROYAL SOCIETY OF CHEMISTRY

PAPER

View Article Online
View Journal | View Issue

Cite this: J. Mater. Chem. A, 2023, 11, 11288

A conformal van der Waals graphene coating enabled high-performance piezo-ionic sensor for spatial, gesture, and object recognition†

Ziqi Li, [ab] Andrew Balilonda,[a] Wen Mei,[a] Wenbo Li[a] and Wei Chen *[abc]

Transforming mechanical forces into electrical signals is vital in self-powered strain sensors. Compared to piezoelectric materials, piezo-ionic materials show great potential in self-powered strain sensors because of the passive and direction identification characteristics arising from the ion gradient under pressure. However, the low signal output (less than 5 mV) of piezo-ionic sensors might be influenced by the bioelectricity when used in practical applications. In addition, the normally used metal electrodes face fracture under high and long-term strain. Here, we used a dry coating method to prepare highly conformal, highly electrically conductive (minimum sheet resistance of 16 ohm sq^{-1}), and highly deformed graphene electrodes with a van der Waals (vdW) structure. Such conformal vdW graphene (vdWGR) electrodes could enhance the signal output to 90.3 mV and resist a large strain of 50% bending variation with 10 000 cycles, avoiding bioelectricity interference and electrode fracture during use. Interestingly, the vdWGR-assisted piezo-ionic sensor exhibited a special "bouncing back" peak when touched by soft objects, which could be utilized for object recognition. We demonstrated its applications in spatial, gesture, and object recognition by utilizing the piezo-ionic strain sensor's differences in the peak value, directionality, and shapes. The preparation method for high-performance vdW graphene electrodes can be extended to other flexible electrodes or electronics. Besides, the piezo-ionic effect identifying the softness or hardness of objects might assist piezo-ionic sensors in more applications.

Received 12th January 2023
Accepted 14th April 2023

DOI: 10.1039/d3ta00215b

rsc.li/materials-a

1. Introduction

Self-powered strain sensors which convert mechanical signals to electrical output show prestigious advantages in motion detection,[1] human–machine interface,[2] and health care[3] because of the portability and direct signal output, rather than conventional capacitive[4] and resistive[5,6] strain sensors that require extra power supplies. Currently, self-powered sensing materials are mainly based on the piezoelectric effect,[7] such as zinc oxide,[8] polyvinylidene fluoride,[9–11] and poly(L-lactic acid).[12] These materials convert mechanical force to electrical signals (potential or current or both), which can generate electricity and be used for self-powered sensing. Such materials encounter difficulties when recognizing directions, *e.g.*, distinguishing upward- or downward-bending. Although a bidirectional identification can be realized through asymmetric structure designs,[13,14] the recognition of multiple directions and even spatial orientation remains a challenge and limits the applications in motion detection. Therefore, developing strain sensors which are self-powered and with spatial recognition capability is of great importance.

Piezo-ionic materials, similar to piezoelectric materials, can also generate electricity because of the ion movement or gradient instead of electron movement under pressure.[1,2,15–18] Compared to piezoresistive, capacitive, and piezoelectric materials, piezo-ionic materials exhibit advantages in direction identification, passive sensing, and fast response from the electrical signals directly related to pressure.[1,19] Although piezo-ionic materials have already been used for sensing in recent years, the signal output still faces a low output value (usually lower than 5 mV) and might be influenced by bioelectricity or other charged objects in practical applications.[1,17,19] Besides, flexible and durable electrodes are as important as the steady signal output because of the strain and pressure applied. Current electrodes are mainly metals, carbon nanotubes, and graphene, which may lack scalable production, have low strain bearing, and easily fracture during use.[20,21] Thus, improving the signal output and finding flexible and durable electrodes are very important in piezo-ionic sensing.

vdW thin films are composed of two-dimensional (2D) materials limited by vdW forces.[22–24] The composed 2D

[a]Research Centre for Smart Wearable Technology, School of Fashion and Textiles, The Hong Kong Polytechnic University, Hung Hom, Kowloon, Hong Kong, 999077, People's Republic of China. E-mail: weii.chen@polyu.edu.hk

[b]The Hong Kong Polytechnic University, Shenzhen Research Institute, Shenzhen, 518057, People's Republic of China

[c]School of Materials Science and Engineering, Zhejiang Sci-Tech University, Hangzhou, 310018, People's Republic of China

† Electronic supplementary information (ESI) available: Fig. S1–S15 and Video 1. See DOI: https://doi.org/10.1039/d3ta00215b

materials possess micro-scale lateral dimensions and nano-scale thickness, forming highly compact vdW films with dangling-bond-free interfaces, flexibility, and a negligible transport barrier. The large width-to-thickness ratio of 2D nanosheets lowers the number of in-plain grain boundaries and decreases the carrier transport barrier—besides, the strong vdW forces with broad-area plane-to-plan attraction result in superb mechanical strength. Thus, vdW thin films or coatings possess excellent mechanical properties and electrical conductivity. All the characteristics of vdW thin films make them promising electrodes for piezo-ionic strain sensors.

In this research, we used a dry coating method to prepare a vdWGR electrode coating directly onto a piezo-ionic sensor. The direct preparation enabled the vdWGR to be conformal with the sensor material, which was limited by the intermolecular force. In addition, the binder and solution-free preparation make the vdWGR electrode has a low sheet resistance of a low sheet resistance of 16 ohm sq^{-1}, a low interface impedance of 4.12 ohm, and 100% conductivity after 10,000 times of bending. Such a vdW coating not only acts as an excellent electrode for strain sensors but also keeps conformal with the sensor surface, enhancing the maximum signal output from 7.2 mV to 90.3 mV and decreasing the response time from 100 ms to 50 ms. In addition, a mask method enables vdW graphene to be coated into any patterns such as strips, sheets, and arrays, facilitating multiple sensing modes, such as bending, touching, or a mixture of these modes. Interestingly, the piezo-ionic sensor could recognize soft and hard objects by identifying the signal shapes. Using this vdW graphene-enhanced piezo-ionic sensor, we demonstrated its applications in spatial recognition, gesture recognition, and object recognition based on the peak value difference, directionality, and shape difference. It is believed that the preparation method for high-performance graphene electrodes could be broadened to other flexible electrodes or electronics. Besides, the discovery of the piezo-ionic effect identifying the softness or hardness of objects is regarded to inspire tactile sensing and human-body interface.

2. Results and discussion

2.1 Piezo-ionic effect

Piezo-ionic materials mainly include ionic polymers or ionic hydrogels, either for sensing,[1,2] electricity generation,[25] mechanoreceptors,[16] or luminescence.[26] In this research, Nafion® 117,

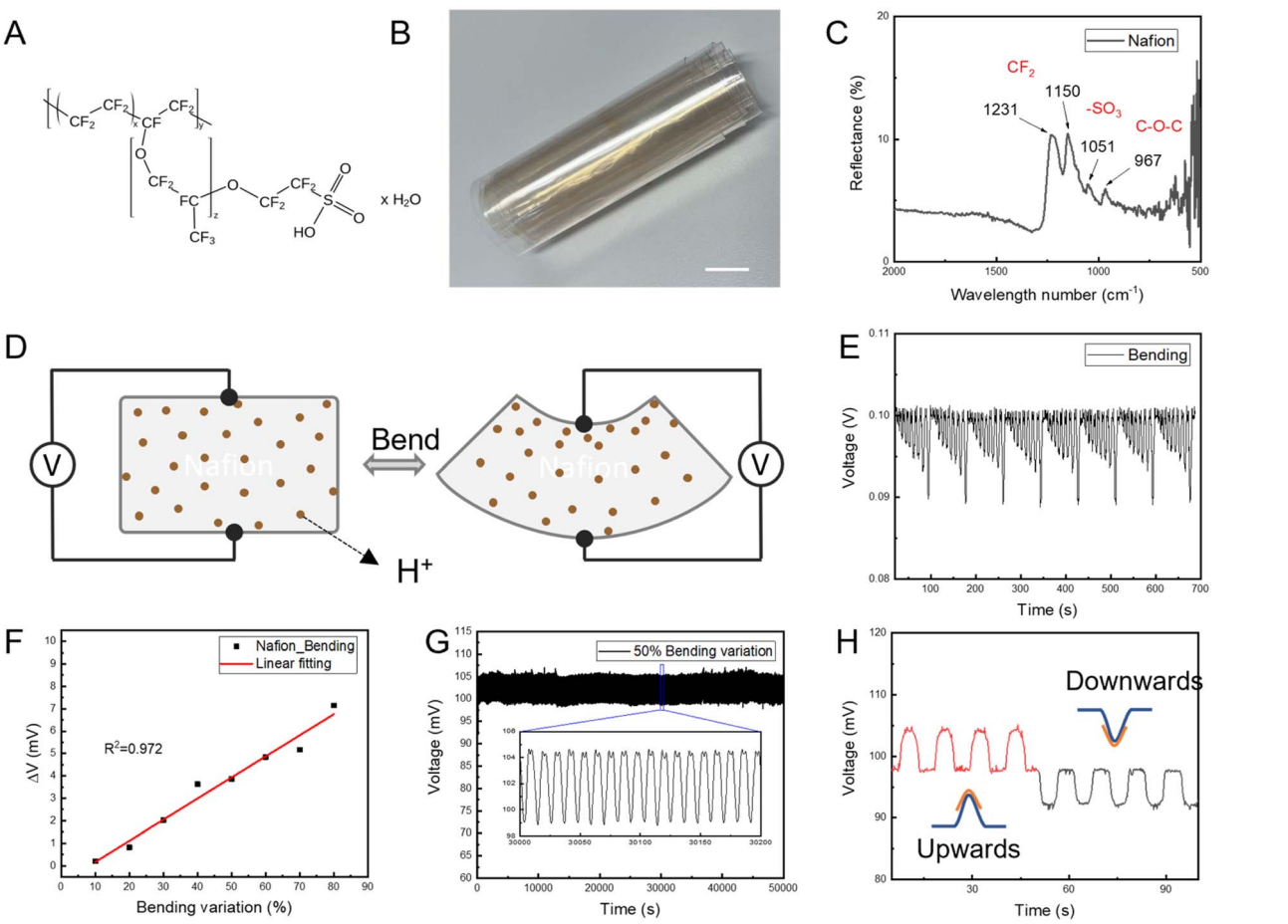

Fig. 1 Piezo-ionic effect: (A) chemical structure of Nafion®, (B) photo of Nafion films, scale bar, 1 cm, (C) FTIR spectrum of Nafion, (D) schematic of ion motion in the Nafion sensor under reversible bending, (E) voltage signal output of the Nafion sensor under the bending variation of 10–90%, (F) linear fitting curve of the voltage output and bending variation of the Nafion film sensor, (G) voltage output of the Nafion bending at 50% bending variation for 10 000 times, and (H) direction difference of the signal output under upwards and downwards bending.

a commercial product designed for fuel cell separators, was chosen as the piezo-ionic sensor due to steady signal output from the uniform structure and smooth surface for electrode integration. Nafion is an ionic polymer with a comb-like structure made of fluorocarbon monomer as a backbone upon which the sulfonic acid terminated perfluoro vinyl ether monomers are decorated as pendants (schematic in Fig. 1A). Visually, it is a transparent thin film with a smooth surface (Fig. 1B). Chemical bonds were determined by Fourier transform infrared (FTIR) spectroscopy. Absorption peaks demonstrating CF_2, CF_2, $-SO_3$, and C–O–C were observed at 1231, 1150, 1051, and 967 cm^{-1}, respectively (Fig. 1C). The polymer membrane contains mobile hydrated cations (protons, H^+) and the cations move in the comb-like structure under stimulation, resulting in an imbalance of the ion gradient and thus the potential difference was produced at different positions (Fig. 1D).

The piezo-ionic effect of Nafion was determined. With copper conductive tapes adhered onto both sides of the Nafion film working as electrodes, the voltage outputs were tested under a series of bending variations from 10% to 90% (testing methods and schematic in Fig. S1†). The ionic polymer could respond to all bending variations, and the voltage output increased with the bending variation increased (Fig. 1E). A linear coefficient of 0.972 and Pearson's coefficient of 0.986 were found when the bending variation was below 80%, confirming the piezo-ionic effect and good linearity working as strain sensors (Fig. 1F). The signal output was measured under 50% bending variation 10 000 times to weigh the stability of Nafion as a strain sensor. There was 0% signal attenuation after 10 000 times, maintaining a potential difference of 4.7 mV (Fig. 1G). The directionality of Nafion was verified, as demonstrated in Fig. 1H. Relative to the baseline, a bend in the opposite direction produced a signal in the opposite direction but the signal peaks remained the same. Besides, the signal outputs of the piezo-ionic sensor in one-electrode mode at different connecting positions were tested, exhibiting the same

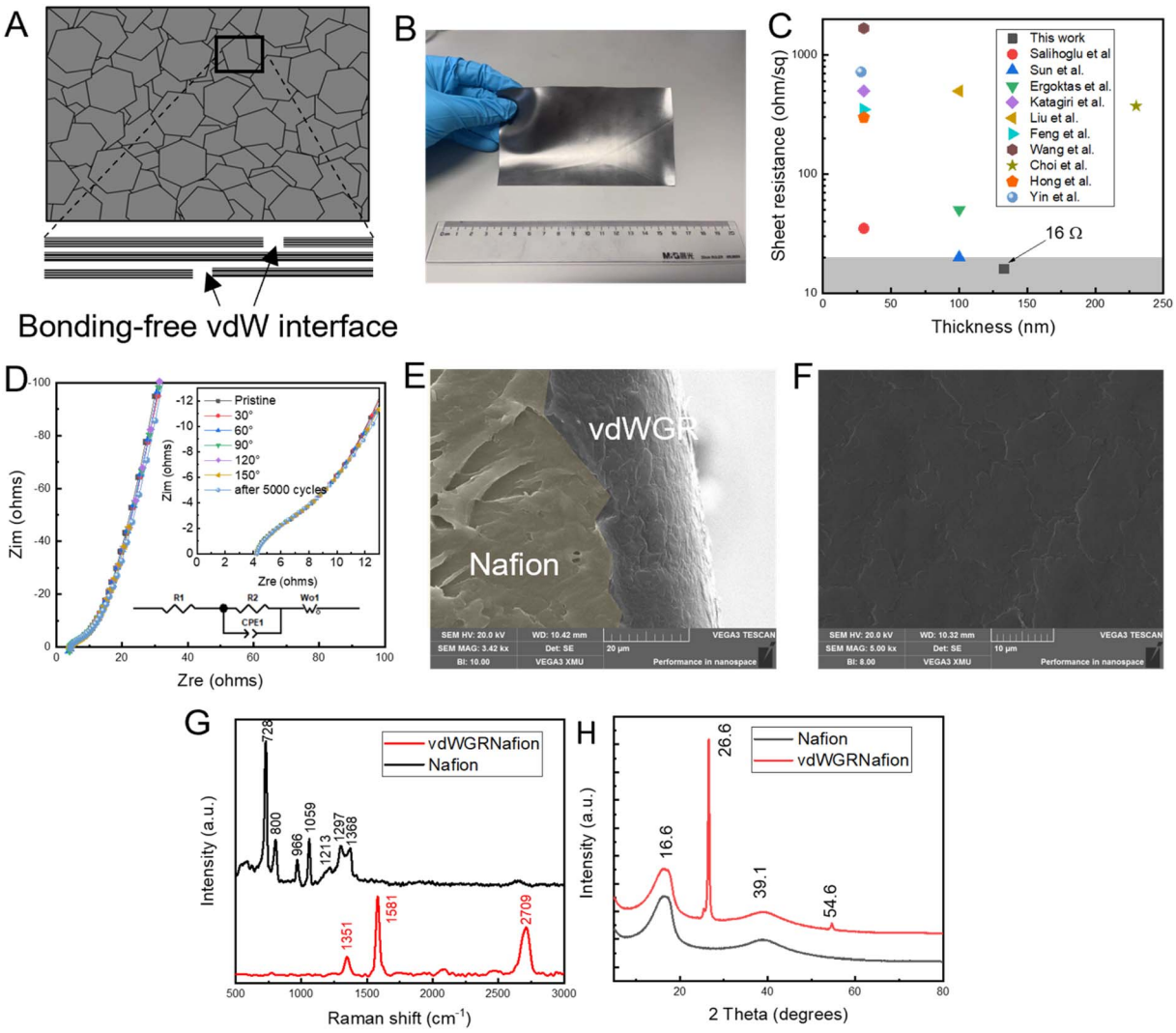

Fig. 2 vdWGR electrode coating: (A) schematic of the vdWGR electrode from top and side views, (B) photograph of the piezo-ionic sensor with vdWGR arrays and sheet resistance of vdWGRN by a four-point method, scale bar, 1 cm, (C) sheet resistance of vdWGR compared to other graphene films,[33–42] (D) Nyquist plots of vdWGRN bending at 0°, 30°, 60°, 90°, 120°, and 150°, and bending after 5000 cycles at 60°, SEM images of vdWGRN from the (E) side view and (F) top view, (G) Raman spectra of Nafion and vdWGRN, and (H) XRD spectra of Nafion and vdWGRN.

signal peak value with the same bend (Fig. S2†). The results indicated that there were still potential differences under all testing conditions, suggesting that the ionic polymer can be used as self-powered strain sensors even with one electrode connection.

2.2 Conformal and highly electrically conductive vdWGR electrodes

The intrinsic excellent electrical conductivity and mechanical properties of the vdW structure make vdW films or coatings good candidates for flexible electrodes. The layer-by-layer structure and bonding-free vdW interface result in negligible transport barriers and high flexibility (Fig. 2A). In this research, a dry coating method was used to prepare vdWGR electrodes. First, a polymer carrier film was chosen to adsorb the graphene nanosheets. Here, nitrile butadiene rubber (NBR), polyethylene, and polypropylene could be used as the polymer carriers. After dragging the polymer carrier with a horizontal force onto the sensor substrate, the graphene nanosheets can be transferred from the polymer carrier to the sensor. Due to the comparable surface energies of graphene nanosheets (35–115 mJ m^{-2}) and Nafion films (14.2 mJ m^{-2}), the layer-by-layer structure of graphene nanosheets is easily formed.[27–29] By repeating the process, graphene nanosheets accumulated onto the Nafion surface, and a vdWGR electrode-assisted Nafion sensor (vdWGRNS) was obtained. It is worth mentioning that the thickness of the vdWGR coating cannot grow infinitely because of the restriction of shear failure.[30] When the loading weight of graphene nanosheets reached 77 mg m^{-2}, no more graphene can be loaded and the sheet resistance of vdWGR reached the minimum (Fig. S3†). As measured by a four-point method, the sheet resistance of vdWGR could reach a minimum value of 16 ohm sq^{-1} and an average value of 52.3 $\pm$ 10.3 Ω sq^{-1} (Fig. 2B and ESI Video 1†). To the best of our knowledge, the as-prepared vdWGR electrode has the lowest sheet resistance among current multilayer graphene films compared to reduced graphene oxide films made by spin coating, electrochemical exfoliation, vacuum filtration, *etc.*[31–42] Compared with CVD-grown graphene films, the sheet resistance is comparable (Fig. 2C). The ultrahigh electrical conductivity result from the vdW structure and the pure layer-by-layer graphene interlayer structure with no impurities, enabling it to work as a high-performance electrode. Besides, the vdWGR electrode adhered to the sensor body tightly under large bending angles, indicating that it is an excellent conformal and flexible electrode (Fig. S4†). Electrochemical impedance spectroscopy (EIS) was used to determine the interfacial impedance of vdWGR and Nafion, which can be used to evaluate the conformality of electrodes on flexible sensors. EIS of the vdWGR electrodes under various bending angles was tested and the Nyquist plots are shown in Fig. 2D. The equivalent circuit diagram was demonstrated and the initial impedance (R_1) of vdWGR was simulated to be 4.17 ohm. The Nyquist plots do not differ much under various bending angles and after long-term bending, indicating the dynamic conformality of the vdWGR coating and the sensor. The long-term stability of vdWGR was tested (Fig. S5†). After 10 000 cycles of large bending, the graphene electrode retains its original conductivity. Also, nearly no morphology changes were found after long-term bending (Fig. S6†). The dry coating method which was binder- and solution-free provided a clean and facile solution for electrode coating preparation, and nonchemical residues make the electrode highly electrically conductive. Besides, compared with preparing an electrode film and then integrating it with the sensor, directly preparing the electrode onto the sensor body endows the interface with low impedance.

The vdW structure was confirmed by scanning electron microscopy (SEM), with graphene nanosheets covered on the sensor's surface conformably in a layered structure with a thickness of 142 nm (Fig. 2E, F and S7†). Spectral tests, including FTIR, Raman, and X-ray diffraction analysis (XRD), were performed to determine the vdWGR electrode coating. Mid-infrared measurements with quantitative functions were used to measure the reflectance of vdWGR. No obvious absorption peaks were observed at the five random positions (Fig. S8†), indicating that the graphene coating covered the Nafion. All testing positions exhibited almost consistent reflectance spectra, demonstrating the uniformity of the vdWGR coating. The emissivity of the structure, calculated from the reflectance and transmittance of vdWGR (Fig. S9†), is 0.54, which is comparable to the thickness of a 100-layer graphene film and in agreement with a thickness of 100–150 nm.[41] The obtained vdWGR coating possesses comparable thickness and conductivity to graphene prepared by a CVD method. However, it performs better in terms of preparation cost, flow, and mechanical fracture resistivity. Fig. 2G shows the Raman spectra of Nafion and vdWGR-coated Nafion (vdWGRN). Peaks observed around 1059, 966, and 800 cm^{-1} originated from the stretching vibrations of S–O, C–O, and S–C in the Nafion side chains. Peaks of asymmetric and symmetric stretching vibrations of CF_2, which occupies a large portion of the ionomer, were observed around 1213 and 728 cm^{-1}, respectively. The C–C single bond peaks were observed around 1297 and 1368 cm^{-1}. The Raman spectrum of the Nafion ionomer is consistent with previous reports.[43] After the graphene was coated, three new peaks were observed at 1351, 1581, and 2709 cm^{-1}, demonstrating graphene's D, G, and 2D peaks. The characteristic peaks of Nafion cannot be observed, demonstrating that the Nafion was fully covered by graphene. Besides, the intensity ratio of D peak to G peak ($I_D/I_G = 0.20$) is extremely low, indicating the low defect of the vdW graphene coating. Fig. 2H shows the XRD results of Nafion with only two diffraction peaks at 17.5° and 39°, which can be attributed to the semi-crystallinity of the perfluorocarbon chains of the ionomer.[44] After coating, two diffraction peaks at 26.2° and 54.6° were observed, which contributed to the C002 and C004 crystalline in the graphite structure. No extra diffraction peaks proved that there are no impurities in vdWGRN.

2.3 Bending

Due to the large area of interconnected two-dimensional nanosheets, vdWGR maintains excellent electrical

conductivity, dynamic conformality, and mechanical performance under reversible strain (Fig. 3A). The vdWGR coating and Nafion attracted to each other by intermolecular forces maintain conformality and low interface impedance under strain. Under a 50% bending variation, the vdWGR could enhance the voltage output from 4.2 mV to 55.3 mV without changing the signal shape (Fig. 3B). The sensing performance of vdWGRNS under 10–80% bending variation was tested (Fig. S10†). The potential difference remained linearly increasing with the bending variation with a maximum signal output of 90.2 mV. Compared with a pure Nafion sensor (NS), the vdWGRNS enhanced the electrical output more than 10 times, as shown in Fig. 3C. Compared with current existing metal-, carbon nanotube- (CNT-), and reduced graphene oxide- (RGO-) based electrodes, vdWGR exhibited significantly higher piezo-ionic output which effectively avoided bioelectric interference (Fig. 3D).[1,19,45] The sensitivity of sensors with graphene electrode coatings has been enhanced. As seen in Fig. 3E, the transient response time was reduced from 100 ms to 50 ms, comparing the NS and vdWGRNS, suggesting that the conformal electrodes could also enhance the response. To explore the effect of a vdWGR electrode coating on the sensor's recovery capability, the bending and recovery times at a 50% bending variation were tested (Fig. 3F). The response and recovery times of the vdWGRNS were 2.21 s and 2.23 s, similar to those of the NS with the values of 2.25 and 2.21 s. The result shows that there is little impact of the vdWGR electrode on the recovery ability.

2.4 Touching

Tactile sensors play an important role in intelligent systems such as wearable devices, medical treatment, artificial limbs, and robotics.[46,47] The piezo-ionic effect is produced by the ion gradient under pressure, allowing it to function as a tactile sensor (Fig. 4A). As illustrated in Fig. 4B, the vdWGR electrode was created on one side of Nafion using the mask method. The constructed electrode in the direction perpendicular to the applied force might receive the signal directly. We measured the signal output of the NS and vdWGRNS, respectively (Fig. 4C). Without the vdWGR electrode, the tactile sensor shows no obvious potential output under various pressure with a maximum signal output of 2.8 mV under 50 N (1.95 cm^2 contacted area, stainless steel accessory). With the vdWGR electrode, the signal output increased with pressure and reached 61 mV under 50 N pressure. The significant difference revealed that the vdWGR electrodes played a role in enhancing the tactile sensor signals. In addition, vdWGRNS was also found to have different signal outputs when recognizing soft and hard objects. We tested the signal of vdWGRNS by hard (stainless

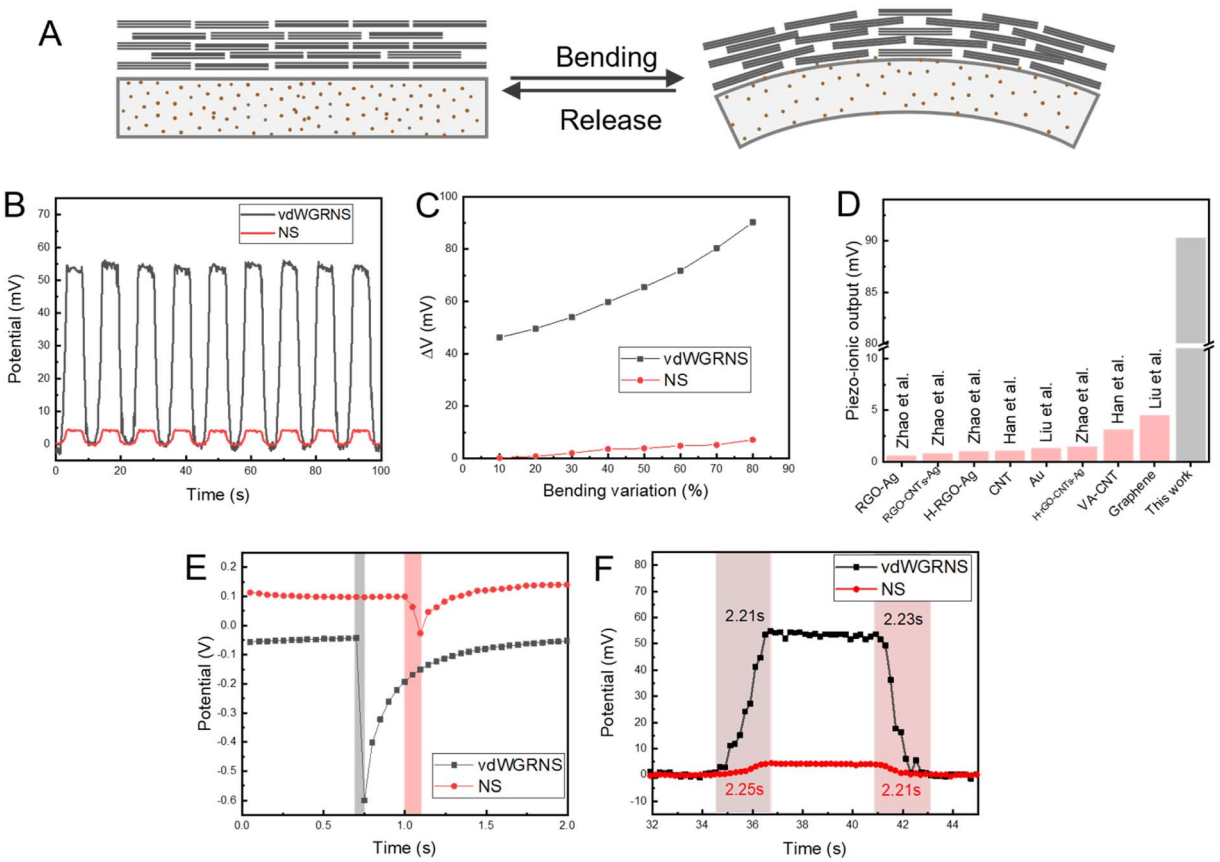

Fig. 3 vdWGRNS for bending: (A) schematic of the vdWGR electrode-assisted piezo-ionic sensor under reversible bending, (B) voltage output of the vdWGRNS and NS under 50% bending variation, (C) voltage output of the vdWGRNS and NS under the bending variation of 10–80%, (D) the piezo-ionic voltage output of the vdWGR-assisted sensor compared to other electrode materials, (E) transient response time of the vdWGRNS and NS, and (F) bending and recovery response of the vdWGRNS and NS under a 50% bending variation.

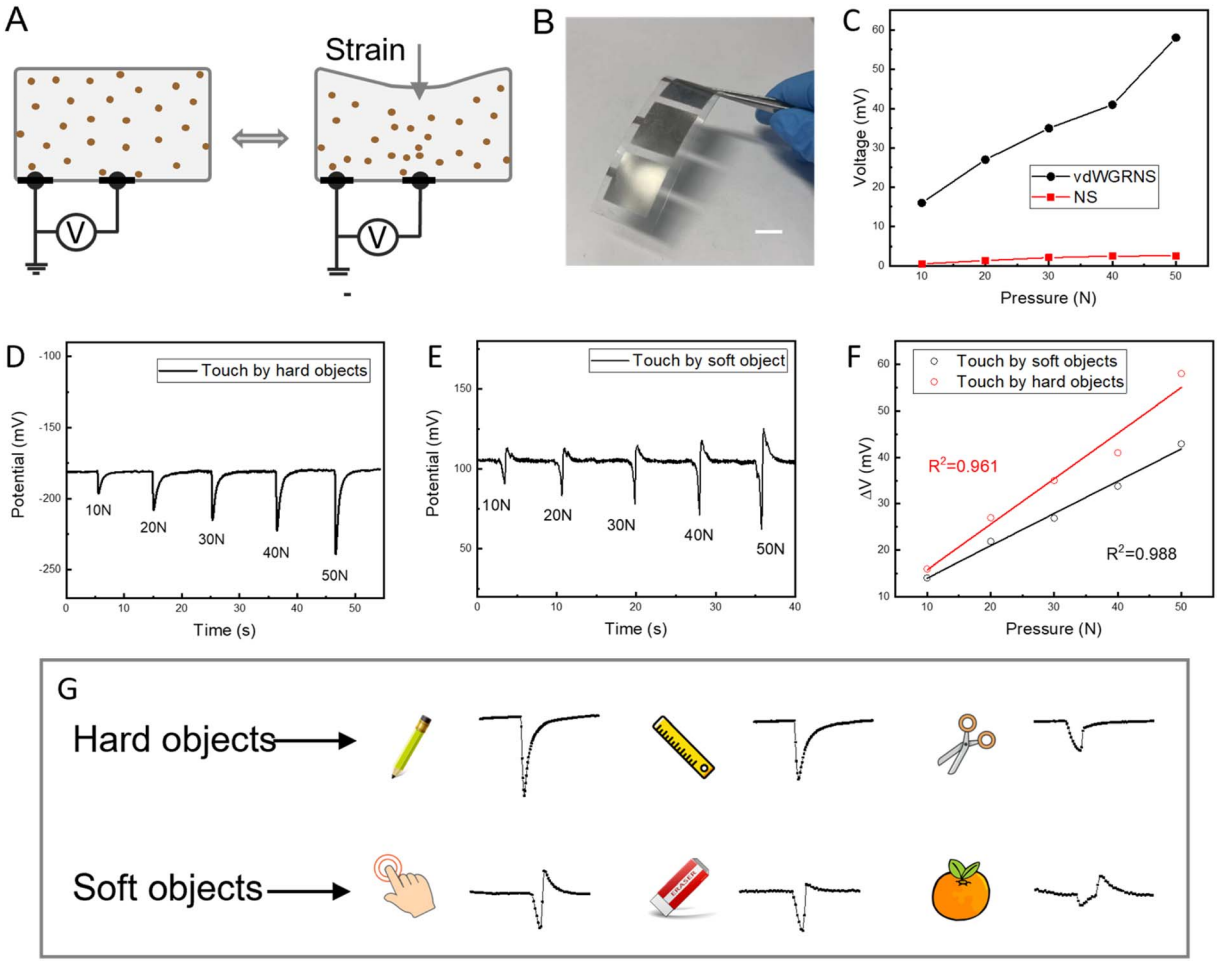

Fig. 4 vdWGRNS for touching: (A) schematic of the piezo-ionic sensor with touching or pressing mode, (B) photograph of the vdWGR electrode coating on one side of the piezo-ionic sensor, (C) comparison of the signal response of the NS and vdWGRNS, (D) signal response of vdWGRNS under pressure from 10 N to 50 N of the stainless steel accessory, (E) signal response of vdWGRNS under pressure from 10 N to 50 N of an accessory wrapping by leather, (F) electrical potential of the vdWGRNS touched by soft and hard objects under the pressure of 10–50 N and corresponding linear fitting curves, and (G) demonstration of signal shapes of vdWGRNS touched by soft object and hard objects.

steel accessory) and soft (leather wrapping the accessory) touches under 10–50 N forces, as illustrated in Fig. 4D and E. When touched by hard objects, the signal output increased with applied force and exhibited a sharp response under pressure of a testing machine. When touched by soft objects, the signal output exhibited "bouncing back" peaks with potential decreased first and then increased when compared with the baseline. The signal output of vdWGRNS under the instant touch of a human finger (pressure around 30 N, measured with a dynamometer) was also tested (Fig. S11†). The potential at the measuring point increased first and then decreased, forming two signal peaks. The sensor's electrical potential dropped by about 26.4 mV when the pressure was applied. With the release of pressure, it increased to 39 mV and then decreased back to the initial potential. Besides, the time to reach the maximum signal value of vdWGRNS touching soft objects (0.69 s) was a little bit longer than touching hard objects (0.21 s). The comparison of the potential change and linear fitting curve of the vdWGRNafion tactile sensor by soft and hard objects is illustrated in Fig. 4F. Linear coefficients of 0.988 and 0.961 demonstrated that the vdWGRNS could be used as a tactile sensor. We further tested some objects with obvious "soft" and "hard" characteristics and found that the typical hard objects possess one peak and typical soft objects possess "bouncing back" peaks (Fig. S12†). The recognition of soft and hard objects by signal peak identification is realized through the vdWGR for piezo-ionic sensors, although it is hard to achieve specific object recognition at this stage.

A series of soft objects (*e.g.*, human fingers, erasers, and fruits) and hard objects (*e.g.*, pens, rulers, and scissors) were used to test the signal shapes. Soft objects' touching caused "bouncing back" peaks, while hard objects caused only one sharp peak (Fig. 4G). We think that the "bouncing back" phenomenon of touching soft objects was caused by the interaction between the soft sensing material and the soft objects, which may come from the elasticity of the materials. Under elastic stress, the cations' gradient or movement produced by the piezo-ionic effect might bounce back.[48] Therefore, the electrical signal will bounce back as the ions' gradient or movement bounces back. By contrast, when a soft sensor

touches a hard object, there is only a deformation process without a rebound. Thus, when the force is released, the ionic polymer returns to its initial state, causing the signal to return to its initial value.

2.5 Spatial recognition, gesture recognition, and object recognition

Based on the characteristics of peak value differences in bending and touching mode, different signal directions, and

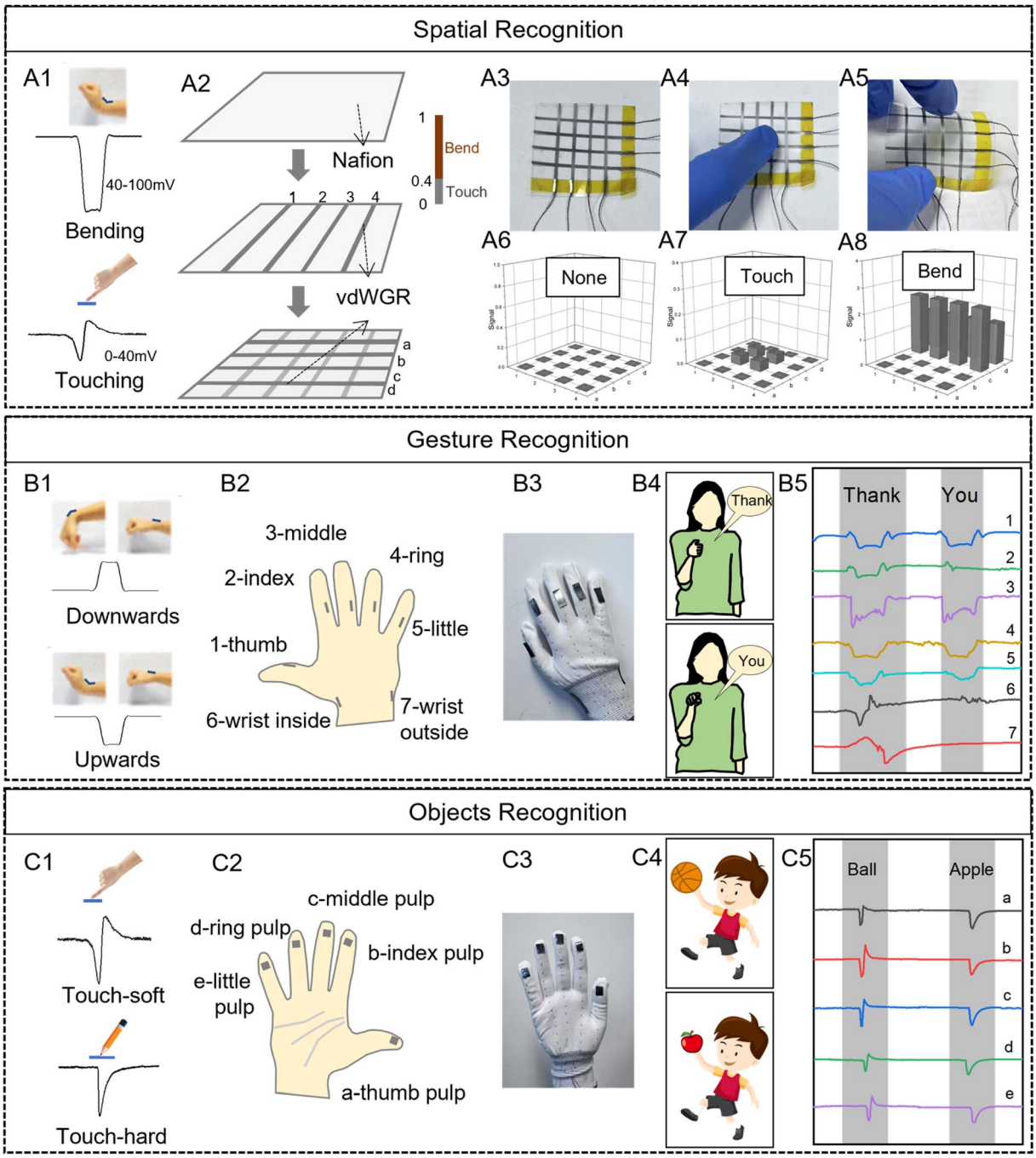

Fig. 5 Applications of the vdWGRNafion piezo-ionic sensor. Spatial recognition: (A1) demonstration of the sensor signals in bending and touching modes, (A2) schematic of constructing vdWGR electrode arrays on both sides of the sensor and index indicator of touching and bending response, pictures of the sensor in (A3) plain, (A4) touch, and (A5) bend modes, and corresponding signal outputs of the sensor in (A6) plain, (A7) touch, and (A8) bend modes. Gesture recognition: (B1) demonstration of gestures and signals in downwards and upwards bending, (B2) sensor locations on the wrist inside, wrist outside, thumb, index, middle, ring, and little fingers, (B3) picture of the smart glove, (B4) hand gesture of "thank you," and (B5) signals of the sign language of "thank you." Objects recognition: (C1) demonstration of gestures and signals touching by soft objects and hard objects, (C2) sensor locations on the thumb, index, middle, ring, and little finger pumps, (C3) photograph of the robotic glove with the sensors, and (C4) schematic and (C5) signals of the hand grasping a basketball and an apple.

shape differences when touching soft and hard objects, we demonstrated three application scenarios of vdWGRNS in spatial recognition, gesture recognition, and object recognition, respectively. The signal value of vdWGRNafion under a normal touch of the human hand (~20 N) is about 30 mV, much lower than the maximum signal value of the sensor under the bending state (100 mV, Fig. 5(A1)). Four vdW graphene stripes were prepared on each side of the piezo-ionic film, as illustrated in Fig. 5(A2). Utilizing the peak value difference, the output signal can determine whether the sensor is bent or touched. The signals from each channel are converted into a matrix with an index of 0 to 1, converting from 0 to 100 mV. Various modes, including a freestanding sensor film (Fig. S13†), touch at one point (Fig. S14†), and bending (Fig. S15†), were tested and demonstrated with a visual matrix (Fig. 5(A3–A8)).

vdWGRNS can recognize the direction when bending downwards or upwards, making the wrist pronation and extorsion identified from the signal direction (Fig. 5(B1)). Utilizing the signal direction and signal shape difference, a smart glove for gesture recognition was demonstrated. As illustrated in Fig. 5(B2), seven bending sensors were located on the five finger joints (thumb, index, middle, ring, and little) and two wrist positions (inside and outside). The glove is shown in Fig. 5(B3). When a finger joint bends, the adhered sensor bends accordingly, with a simultaneous potential change detected. The language actions of "thank you" were demonstrated with potential signals (Fig. 5(B4 and B5)). The hand gesture can be identified by identifying the shape of signal peaks at different locations. Besides, as mentioned in Section 2.3, the bending variation can be identified by weighing the signal value. Such motion detection and bending variation detection capability enable the piezo-ionic sensor to communicate with deaf or hard of hearing people who do not speak verbally in sign language recognition.

The human–machine interface faces scenarios to identify objects, such as a robotic hand, to identify the object's hardness. When a soft object comes into contact with the pressure ion sensor, it shows a signal peak with a rebound (two signal peaks, Fig. 5(C1)). When touched by a hard object, it exhibits a sharp signal peak. This allows vdWGRNafion sensors to be used in robotic hands to identify objects. As demonstrated in Fig. 5(C2), five piezo-ionic sensors with the dimensions of 5 mm × 5 mm were placed on the belly of each finger. The glove for the robotic hand is shown in Fig. 5(C3). When the robotic hand touches a basketball (soft object, Fig. 5(C4)), all five signal channels show rebound touch signals. When the robotic hand picks up an apple (hard object), the signal representing the hard object is fed back to the response signal channel (Fig. 5(C5)). Although vdWGRNafion piezo-ionic sensors cannot identify specific object types, the preliminary identification of soft or hard objects provides the basis for studying human–machine interfaces.

3. Conclusions

To conclude, we coated graphene electrodes with a vdW structure directly onto a self-powered piezo-ionic (Nafion) sensor to enhance signal output and apply it to various sensing and human–machine interface scenarios. The dry coating method is facile, binder- and solution free, and conformal, which might be extended to other flexible electrodes and electronics. Due to the conformal vdW graphene electrode layer being limited by intermolecular forces, the impedance in the electrode layer and piezo-ionic material layer is very low, resulting in enhanced electrical signals of the sensor (maximum value of 90.2 mV) and sensitivity (response time of 50 ms). The vdWGR electrode was highly conductive (16 ohm sq^{-1}) and resisted a large bending variation of 50% of 10 000 cycles. Besides, the vdW graphene electrodes can be designed into any pattern, such as strips, squares, or arrays, enabling both bending sensing and tactile sensing. Based on the vdWGRNS, we demonstrated its application in spatial, gesture, and object recognition using the peak value difference, directionality, and shape difference touching by soft and hard objects. Utilizing the peak value difference of vdWGRNS under bending and touching, spatial recognition can be realized by signal identification. Utilizing the directionality and linear coefficient of the vdWGRNS, a smart glove gesture recognition for deaf or hard of hearing people who do not speak verbally was realized. Utilizing the signal shape difference of the sensor to hard and soft objects, an initial object recognition capability is demonstrated. Although identifying the object type cannot be realized currently, this study is considered to provide a research basis and technical development direction in the scientific research of self-powered piezo-ionic sensors.

4. Experimental section

4.1 Materials

Nafion® 117 films composed of sulfonated tetrafluoroethylene-based fluoropolymer–copolymer purchased from Dupont were used as the piezo-ionic sensor materials. Graphene nanosheets with 5–8 layers, 95% carbon content, and 3–10 μm lateral diameter were purchased from China Graphene Institute. H_2O_2 (3 wt%) and H_2SO_4 (90 wt%) were purchased from Shanghai Macklin Biochemical Co., Ltd.

4.2 Construction of the piezo-ionic sensors

The Nafion® 117 film underwent a pretreatment before construction into the integrated sensor: 5% wt H_2O_2 boiled for 1 h at 80 °C, followed by washing with deionized water and keeping for 30 min, followed by boiling 5% wt H_2SO_4 for 1 h at 80 °C, followed by washing with deionized water and drying overnight. The vdW graphene electrode coating was prepared through a mechanical adhesion method. Firstly, moderate graphene nanosheets adhered onto an NBR polymer carrier film. Then, the graphene nanosheet side was dragged by a horizontal force paralleled to the Nafion film. Graphene nanosheets were separated from the NBR film and transferred to the Nafion film. By repeating the adhesion–dragging–separation process, vdW graphene-coated Nafion was obtained finally. The vdW graphene coating worked as an electrode, and conductive copper tape was pasted to the constructed sensor as an external electrode connecting to a multi-meter for testing.

4.3 Mechanical tests

The piezo-ionic sensor was pasted onto a motorized translation stage (Beijing Optical Century Instrument Co., Ltd., MTS121) with an insulation paste. The free length of the sample was 30 mm, and the testing length of the sample was 10 mm (as demonstrated in Fig. S1†). The deformation of the samples was controlled by using a step motor. Tactile sensing was tested by using a pull-and-push dynamometer (HP-100, Adelberg Instrument Co. Ltd). All the output electrical signals were recorded by using a Keithley 2400 Source Meter.

4.4 Characterization

Surface morphologies were determined by SEM (Tescan VEGA). The sheet resistance of the vdW graphene electrode coating was tested by using a KDY-1 four-probe square resistance tester. Spectral reflectance and transmittance in the mid-infrared wavelength range were characterized by using an FTIR (Spectrum 100, PerkinElmer) equipped with a diffuse gold integrating sphere. Raman was performed under a 532 nm laser with a Renishaw Micro-Raman Spectroscopy System. XRD was performed with a Rigaku SmartLab 9 kW. EIS was recorded in the frequency range of 0.01–100 000 Hz, performed by using a Versa STAT3 electrochemical workstation.

Author contributions

Z. L. and W. C. conceived the idea and designed the experiments. Z. L. prepared the samples, fabricated the devices, and performed the measurements. All authors contributed to the discussion, preparation, and revision of the manuscript.

Conflicts of interest

The authors declare no conflict of interest.

Acknowledgements

The authors would like to thank the Shenzhen-Hong Kong-Macao Science and Technology Plan Project (SGDX2020110309520101), Research Grants Council of Hong Kong (15302121), National Natural Science Foundation of China (21975214), National Key R&D Program of China (2018YFC2000900), Seed Fund of Research Institute of Intelligent Wearable Systems (CD45), Start-up Fund of The Hong Kong Polytechnic University (BE1H), and Departmental General Research Fund of The Hong Kong Polytechnic University (UAME).

References

1 Y. Liu, *et al.*, Self-Powered Piezoionic Strain Sensor toward the Monitoring of Human Activities, *Small*, 2016, **12**(36), 5074–5080.
2 M. S. Sarwar, *et al.*, Bend, stretch, and touch: Locating a finger on an actively deformed transparent sensor array, *Sci. Adv.*, 2017, **3**(3), e1602200.
3 G. Zhu, *et al.*, Self-powered and multi-mode flexible sensing film with patterned conductive network for wireless monitoring in healthcare, *Nano Energy*, 2022, **98**, 107327.
4 A. Frutiger, *et al.*, Capacitive soft strain sensors *via* multicore-shell fiber printing, *Adv. Mater.*, 2015, **27**(15), 2440–2446.
5 X. Liao, *et al.*, Ultrasensitive and stretchable resistive strain sensors designed for wearable electronics, *Mater. Horiz.*, 2017, **4**(3), 502–510.
6 J. Ren, *et al.*, A graphene rheostat for highly durable and stretchable strain sensor, *InfoMat*, 2019, **1**(3), 396–406.
7 M. T. Chorsi, *et al.*, Piezoelectric Biomaterials for Sensors and Actuators, *Adv. Mater.*, 2019, **31**(1), e1802084.
8 C. Dagdeviren, *et al.*, Transient, biocompatible electronics and energy harvesters based on ZnO, *Small*, 2013, **9**(20), 3398–3404.
9 L. Lu, *et al.*, Flexible PVDF based piezoelectric nanogenerators, *Nano Energy*, 2020, **78**, 105251.
10 A. V. Shirinov and W. K. Schomburg, Pressure sensor from a PVDF film, *Sens. Actuators, A*, 2008, **142**(1), 48–55.
11 Y. R. Wang, *et al.*, A flexible piezoelectric force sensor based on PVDF fabrics, *Smart Mater. Struct.*, 2011, **20**(4), 045009.
12 E. J. Curry, *et al.*, Biodegradable Piezoelectric Force Sensor, *Proc. Natl. Acad. Sci. U. S. A.*, 2018, **115**(5), 909–914.
13 W. Choi, *et al.*, Asymmetric 2D MoS(2) for Scalable and High-Performance Piezoelectric Sensors, *ACS Appl. Mater. Interfaces*, 2021, **13**(11), 13596–13603.
14 X. Liao, *et al.*, Flexible and Highly Sensitive Strain Sensors Fabricated by Pencil Drawn for Wearable Monitor, *Adv. Funct. Mater.*, 2015, **25**(16), 2395–2401.
15 A. Lasheras, *et al.*, Development of novel piezo-ionic/magnetostrictive composites for energy generation systems, *Smart Mater. Struct.*, 2020, **29**(8), 85041.
16 Y. Dobashi, *et al.*, Piezoionic mechanoreceptors: Force-induced current generation in hydrogels, *Science*, 2022, **376**(6592), 502–507.
17 Y. Ming, *et al.*, IPMC Sensor Integrated Smart Glove for Pulse Diagnosis, Braille Recognition, and Human–Computer Interaction, *Adv. Mater. Technol.*, 2018, **3**(12), 1800257.
18 C. Lu, *et al.*, Highly Sensitive Ultrastable Electrochemical Sensor Enabled by Proton-Coupled Electron Transfer, *Nano Lett.*, 2021, **21**(12), 5369–5376.
19 S. Han, *et al.*, Bionic ion channel and single-ion conductor design for artificial skin sensors, *J. Mater. Chem. B*, 2017, **5**(34), 7126–7132.
20 V. B. Mohan, *et al.*, Graphene-based materials and their composites: A review on production, applications and product limitations, *Composites, Part B*, 2018, **142**, 200–220.
21 G. Wang, L. Zhang and J. Zhang, A review of electrode materials for electrochemical supercapacitors, *Chem. Soc. Rev.*, 2012, **41**(2), 797–828.
22 P. Wang, *et al.*, Van der Waals Heterostructures by Design: From 1D and 2D to 3D, *Matter*, 2021, **4**(2), 552–581.
23 Z. Lin, Y. Huang and X. Duan, Van der Waals thin-film electronics, *Nat. Electron.*, 2019, **2**(9), 378–388.
24 J. Zhong, *et al.*, Efficient and scalable synthesis of highly aligned and compact two-dimensional nanosheet films with record performances, *Nat. Commun.*, 2018, **9**(1), 3484.

25 S. Yang, *et al.*, Ionic Hydrogel for Efficient and Scalable Moisture-Electric Generation, *Adv. Mater.*, 2022, **34**(21), e2200693.
26 J. I. Lee, *et al.*, Visco-Poroelastic Electrochemiluminescence Skin with Piezo-Ionic Effect, *Adv. Mater.*, 2021, **33**(29), e2100321.
27 D. K. Paul, *et al.*, Characteristics of Self-Assembled Ultrathin Nafion Films, *Macromolecules*, 2013, **46**(9), 3461–3475.
28 A. Ferguson, *et al.*, The dependence of the measured surface energy of graphene on nanosheet size, *2D Mater.*, 2017, **4**(1), 015040.
29 Z. Li, *et al.*, Scalable van der Waals graphene films for electro-optical regulation and thermal camouflage, *InfoMat*, 2023, e12418.
30 C. J. Castilho, *et al.*, Shear Failure in Supported Two-Dimensional Nanosheet Van der Waals Thin Films, *Carbon*, 2021, **173**, 410–418.
31 Y. Chen, *et al.*, Graphene as a Transparent and Conductive Electrode for Organic Optoelectronic Devices, *Adv. Electron. Mater.*, 2019, **5**(10), 190024.
32 K. Rana, J. Singh and J.-H. Ahn, A graphene-based transparent electrode for use in flexible optoelectronic devices, *J. Mater. Chem. C*, 2014, **2**(15), 2646–2656.
33 Z. Yin, *et al.*, Organic Photovoltaic Devices Using Highly Flexible Reduced Graphene Oxide Films as Transparent Electrodes, *ACS Nano*, 2010, **4**(9), 5263–5268.
34 J. T. Hong, *et al.*, Terahertz conductivity of reduced graphene oxide films, *Opt. Express*, 2013, **21**(6), 7633–7640.
35 Y.-Y. Choi, *et al.*, Multilayer graphene films as transparent electrodes for organic photovoltaic devices, *Sol. Energy Mater. Sol. Cells*, 2012, **96**, 281–285.
36 J. Liu, *et al.*, Multilayer stacked low-temperature-reduced graphene oxide films: preparation, characterization, and application in polymer memory devices, *Small*, 2010, **6**(14), 1536–1542.
37 M. Katagiri, *et al.*, Electrical properties of multilayer graphene interconnects prepared by chemical vapor deposition, in *2013 IEEE International Interconnect Technology Conference - IITC*, 2013.
38 J. Wang, *et al.*, Rod-coating: towards large-area fabrication of uniform reduced graphene oxide films for flexible touch screens, *Adv. Mater.*, 2012, **24**(21), 2874–2878.
39 H. Feng, *et al.*, A low-temperature method to produce highly reduced graphene oxide, *Nat. Commun.*, 2013, **4**, 1539.
40 M. S. Ergoktas, *et al.*, Multispectral graphene-based electro-optical surfaces with reversible tunability from visible to microwave wavelengths, *Nat. Photonics*, 2021, **15**(7), 493–498.
41 Y. Sun, *et al.*, Flexible Mid-Infrared Radiation Modulator with Multilayer Graphene Thin Film by Ionic Liquid Gating, *ACS Appl. Mater. Interfaces*, 2019, **11**(14), 13538–13544.
42 O. Salihoglu, *et al.*, Graphene-Based Adaptive Thermal Camouflage, *Nano Lett.*, 2018, **18**(7), 4541–4548.
43 M. Hara, *et al.*, Temperature dependence of the water distribution inside a Nafion membrane in an operating polymer electrolyte fuel cell. A micro-Raman study, *Electrochim. Acta*, 2011, **58**, 449–455.
44 H. W. Starkweather Jr, Crystallinity in perfluorosulfonic acid ionomers and related polymers, *Macromolecules*, 1982, **15**(2), 320–323.
45 J. Zhao, *et al.*, Passive and Space-Discriminative Ionic Sensors Based on Durable Nanocomposite Electrodes toward Sign Language Recognition, *ACS Nano*, 2017, **11**(9), 8590–8599.
46 Y. Liu, *et al.*, Recent progress in tactile sensors and their applications in intelligent systems, *Sci. Bull.*, 2020, **65**(1), 70–88.
47 Y. Liu, *et al.*, Highly Sensitive Wearable Pressure Sensor Over a Wide Sensing Range Enabled by the Skin Surface-Like 3D Patterned Interwoven Structure, *Adv. Mater. Technol.*, 2022, **7**(12), 2200504.
48 Z. Zhu, *et al.*, Effects of cation on electrical responses of ionic polymer-metal composite sensors at various ambient humidities, *J. Appl. Phys.*, 2016, **120**(8), 084906.